Natural *J*-Coupling Analysis: Interpretation of Scalar *J*-Couplings in Terms of Natural Bond Orbitals

Steven J. Wilkens,[†,||] William M. Westler,[‡] John L. Markley,*[,†,‡] and Frank Weinhold[†,§]

Contribution from the National Magnetic Resonance Facility at Madison, Department of Biochemistry, Theoretical Chemistry Institute, and Department of Chemistry, University of Wisconsin—Madison, 433 Babcock Drive, Madison, Wisconsin 53706

Received May 25, 2001

Abstract: The natural *J*-coupling (NJC) method presented here analyzes the Fermi contact portion of *J*-coupling in the framework of finite perturbation theory applied to ab initio/density function theory (DFT) wave functions, to compute individual and pairwise orbital contributions to the net *J*-coupling. The approach is based on the concepts and formalisms of natural bond orbital (NBO) methods. Computed coupling contributions can be classified as Lewis (individual orbital contributions corresponding to the natural Lewis structure of the molecule), delocalization (resulting from pairwise donor−acceptor interactions), and residual repolarization (corresponding to correlation-like interactions). This approach is illustrated by an analysis of the angular and distance dependences of the contributions to vicinal $^3J_{HH}$ couplings in ethane and to the long-range $^6J_{HH}$ couplings in pentane. The results indicate that approximately 70% or more of the net *J*-coupling is propagated by steric exchange antisymmetry interactions between Lewis orbitals (predominantly σ bonding orbitals). Hyperconjugative σ to σ^* delocalization interactions account for the remainder of the coupling. Calculated pairwise−steric and hyperconjugative−delocalization energies provide a means for relating coupling mechanisms to molecular energetics. In this way, *J*-coupling contributions can be related directly to the localized features of the molecular electronic structure in order to explain measured *J*-coupling patterns and to predict *J*-coupling trends that have yet to be measured.

I. Introduction

The structural information contained in indirect, nuclear spin−nuclear spin scalar couplings (*J*-couplings) has been appreciated since the first work on liquid-state NMR.[1] Not only do *J*-couplings contain information about chemical connectivity, they also contain geometrical information as first shown by Karplus in 1959.[2,3] Scalar couplings also have been exploited as an important mechanism for the transfer of magnetization in modern multidimensional NMR experiments. Despite the ubiquitous nature of *J*-coupling, more can be learned about how the electronic structure of the molecule modulates observed couplings. The goal of this paper is to present a method for connecting the *J*-coupling phenomenon to calculated ab initio and density functional wave functions by means of intuitive chemical bonding concepts.

Unlike most of the other properties of NMR, which can be understood on the basis of semiclassical physics, *J*-coupling is purely a quantum-mechanical phenomenon. Large strides have been made in recent years toward the accurate computation of coupling constants from first principles.[4−16] This paper builds on the single, finite-perturbation methodology first formulated by Pople and co-workers,[17−21] which has been shown to yield accurate results when applied in the framework of modern (hybrid) density functional theory (DFT).[11] Although this

* To whom correspondence should be addressed. E-mail: markley@nmrfam.wisc.edu.

† Graduate Program in Biophysics.

‡ Department of Biochemistry.

§ Department of Chemistry.

|| Current address: Genomics Institute of the Novartis Research Foundation, 3115 Merryfield Row, Suite 200, San Diego, CA 92121-1125.

(1) Emsley, J. W.; Feeney, J.; Sutcliffe, L. H. *High-Resolution Nuclear Magnetic Resonance Spectroscopy*; Pergamon Press: Oxford, 1966.

(2) Karplus, M. *J. Chem. Phys.* **1959**, *30*, 11−15.

(3) Karplus, M. *J. Am. Chem. Soc.* **1963**, *85*, 2870−2871.

(4) Arnold, W. D.; Mao, J. H.; Sun, H. H.; Oldfield, E. *J. Am. Chem. Soc.* **2000**, *122*, 12164−12168.

(5) Arnold, W. D.; Oldfield, E. *J. Am. Chem. Soc.* **2000**, *122*, 12835−12841.

(6) Benedict, H.; Shenderovich, I. G.; Malkina, O. L.; Malkin, V. G.; Denisov, G. S.; Golubev, N. S.; Limbach, H. H. *J. Am. Chem. Soc.* **2000**, *122*, 1979−1988.

(7) Case, D. A.; Scheurer, C.; Bruschweiler, R. *J. Am. Chem. Soc.* **2000**, *122*, 10390−10397.

(8) Cloran, F.; Carmichael, I.; Serianni, A. S. *J. Am. Chem. Soc.* **1999**, *121*, 9843−9851.

(9) Dingley, A. J.; Masse, J. E.; Peterson, R. D.; Barfield, M.; Feigon, J.; Grzesiek, S. *J. Am. Chem. Soc.* **1999**, *121*, 6019−6027.

(10) Fierman, M.; Nelson, A.; Khan, S. I.; Barfield, M.; O'Leary, D. J. *Org. Lett.* **2000**, *2*, 2077−2080.

(11) Onak, T.; Jaballas, J.; Barfield, M. *J. Am. Chem. Soc.* **1999**, *121*, 2850−2856.

(12) Scheurer, C.; Bruschweiler, R. *J. Am. Chem. Soc.* **1999**, *121*, 8661−8662.

(13) Contreras, R. H.; Peralta, J. E. *Prog. Nucl. Magn. Res. Spectrosc.* **2000**, *37*, 321−425.

(14) Del Bene, J. E.; Bartlett, R. J. *J. Am. Chem. Soc.* **2000**, *122*, 10480−10481.

(15) Del Bene, J. E.; Perera, S. A.; Bartlett, R. J. *J. Am. Chem. Soc.* **2000**, *122*, 3560−3561.

(16) Del Bene, J. E.; Perera, S. A.; Bartlett, R. J. *J. Phys. Chem. A* **2001**, *105*, 930−934.

(17) Maciel, G. E.; McIver, J. W., Jr.; Ostlund, N. S.; Pople, J. A. *J. Am. Chem. Soc.* **1970**, *92*, 4151−4157.

(18) Maciel, G. E.; McIver, J. W., Jr.; Ostlund, N. S.; Pople, J. A. *J. Am. Chem. Soc.* **1970**, *92*, 4497−4505.

(19) Maciel, G. E.; McIver, J. W., Jr.; Ostlund, N. S.; Pople, J. A. *J. Am. Chem. Soc.* **1970**, *92*, 4506.

(20) Pople, J. A.; McIver, J. W., Jr.; Ostlund, N. S. *J. Chem. Phys.* **1968**, *49*, 2960−2964.

(21) Pople, J. A.; McIver, J. W., Jr.; Ostlund, N. S. *J. Chem. Phys.* **1968**, *49*, 2965−2970.

10.1021/ja016284k CCC: $20.00
Published on Web 11/06/2001

method only treats the Fermi contact portion of the coupling, previous work strongly suggests that the Fermi contact mechanism dominates.[11,12,14−16] Moreover, the finite perturbation approach provides a simple and efficient context in which to compute and conceptualize *J*-coupling. Other contributions (e.g., spin−dipolar) may be significant for heavy-atom coupling in conjugated systems (especially when it involves at least one fluorine nucleus).[22]

Because nuclear spin orientation information is transferred by the electronic structure to other nuclei in the molecule, empirically determined *J*-couplings speak directly to the nature of the chemical bond. In particular, the ability to measure trans-hydrogen-bond *J*-couplings has added fuel to the debate over the covalent character of hydrogen bonds.[9,23−31] Thus, trans-hydrogen-bond *J*-coupling may yield information that is fundamental to understanding the essential role of hydrogen bonding in biological systems.

In this paper, we present natural *J*-coupling (NJC) as an approach for analyzing scalar couplings based on natural bond orbital (NBO) methods.[32] NJC differs from previous approaches in which computed couplings were related to valence bond order[6] or charge density.[4] NJC calculates the Fermi contact portion of the *J*-coupling constant directly in terms of individual and pairwise (donor−acceptor) NBO contributions. The NBO package includes a suite of methods for describing the *N*-electron wave function $\psi(1,2,...,N)$ in terms of localized orbitals or configurations that are closely tied to chemical bonding concepts.[33,34] Underlying these methods are the sets of localized intrinsic "natural" atomic orbitals (NAOs), bond orbitals (NBOs), and semilocalized molecular orbitals (NLMOs), which are in close correspondence with the Lewis structure representations used by chemists. Both the NBOs and NLMOs are complete and orthonormal, in addition to being optimally chosen with respect to the molecular environment to describe the electron density and other properties in the most rapidly convergent fashion. The populations (or occupancies) of these orbitals are therefore highly condensed into the fewest, most important members (i.e., those corresponding to the Lewis-like bonds and lone pairs of the formal Lewis structure), allowing the remaining contributions to be satisfactorily treated as small corrections by standard perturbative methods. Specifically, we discuss how *J*-coupling, or rather the transfer of spin density, is related to spin hyperconjugative delocalization (by means of 2nd order perturbation analysis) and to wave function antisymmetrization (by means of natural steric analysis, NSA[33]). With these methods, *J*-coupling mechanisms can be related to localized energetics of the molecular electronic structure so as to provide an intuitive understanding of *J*-coupling. The approach also can be used to predict *J*-coupling interactions and to understand the signs and magnitudes of expected couplings as a function of molecular conformation. Proton couplings in aliphatic model systems are used to introduce the concepts of NJC. These concepts can be generalized to a wide range of systems.

Table 1. Summary of the Calculated Contributions to the Vicinal $^3J_{HH}$ Coupling of the Trans Ethane Model (Figure 1B)[a]

	σ_{C2-H1} (/Hz)	σ_{C3-H4} (/Hz)	others (/Hz)	total (/Hz)
Lewis	+5.52	+5.52	−0.06	+10.97
repolarization	−0.07	−0.07	0.00	−0.14
σ_{C2-H1}*		+2.63	+0.56	+3.19
σ_{C3-H4}*	+2.63		+0.56	+3.19
other	−1.05	−1.05	−0.39	−2.49
(total delocalization)	(+1.58)	(+1.58)	(+0.73)	(+3.89)
total	+7.02	+7.02	+0.67	+14.72

[a] Calculation performed at B3LYP/6-311G** with a Fermi contact perturbation of 0.02 au.

Very recently, a closely related form of "natural *J*-coupling analysis" was presented by Peralta, Contreras, and Snyder.[35] Their work is also based on the use of localized NBO/NLMO methods to decompose *J*-coupling and may be considered equivalent to the initial NLMO expansion (eq 5, or the final row in Table 1; see in a later section), which is the first step in the present treatment. While the localized NLMO contributions already provide powerful information about *J*-coupling, we believe that much further information derives from the expansion in Lewis- and non-Lewis-type NBO interactions, which clearly identifies distinct physical contributions of "steric" versus "hyperconjugative" origin. Thus, the present treatment is completely consistent with both the letter and spirit of the previous work[35] but gives a more complete and detailed NBO-based picture of *J*-coupling contributions.

II. Theory

The Hamiltonian describing nuclear spin−nuclear spin scalar coupling in the framework of finite perturbation theory is given by

$$H = H_0 + A_M\mu_M + A_N\mu_N \tag{1}$$

where H_0 is the unperturbed Hamiltonian and μ_M and μ_N are nuclear spin operators. A_M and A_N are, in this case, the Fermi contact terms for nuclei N and M, which have the form[11]

$$A_N = \left(\frac{16\pi\mu_b}{3}\right)\Delta(r_N) \tag{2}$$

where μ_b is the Bohr magneton and $\Delta(r_N)$ is the Fermi contact spin difference density. The latter is given by

$$\Delta(r_N) = \sum_{i,j}\Gamma_{ij}\langle\phi_i|\delta(r_N)|\phi_j\rangle \tag{3}$$

where Γ_{ij} is the ijth element of the one-electron spin density

(22) Peralta, J. E.; Barone, V.; de Azua, M. C. R.; Contreras, R. H. *Mol. Phys.* **2001**, *99*, 655−661.
(23) Dingley, A. J.; Grzesiek, S. *J. Am. Chem. Soc.* **1998**, *120*, 8293−8297.
(24) Cordier, F.; Wang, C. Y.; Grzesiek, S.; Nicholson, L. K. *J. Mol. Biol.* **2000**, *304*, 497−505.
(25) Dingley, A. J.; Masse, J. E.; Feigon, J.; Grzesiek, S. *J. Biomol. NMR* **2000**, *16*, 279−289.
(26) Hennig, M.; Geierstanger, B. H. *J. Am. Chem. Soc.* **1999**, *121*, 5123−5126.
(27) Liu, A.; Hu, W. D.; Qamar, S.; Majumdar, A. *J. Biomol. NMR* **2000**, *17*, 55−61.
(28) Meissner, A.; Sorensen, O. W. *J. Magn. Reson.* **2000**, *143*, 387−390.
(29) Meissner, A.; Sorensen, O. W. *J. Magn. Reson.* **2000**, *143*, 431−434.
(30) Pervushin, K.; Fernandez, C.; Riek, R.; Ono, A.; Kainosho, M.; Wüthrich, K. *J. Biomol. NMR* **2000**, *16*, 39−46.
(31) Wang, Y. X.; Jacob, J.; Cordier, F.; Wingfield, P.; Stahl, S. J.; Lee-Huang, S.; Torchia, D.; Grzesiek, S.; Bax, A. *J. Biomol. NMR* **1999**, *14*, 181−184.
(32) Weinhold, F. Natural Bond Orbital Methods. In *Encyclopedia of Computational Chemistry*; Schleyer, P. v. R., Ed.; Theoretical Chemistry Institute and the Department of Chemistry, University of Wisconsin-Madison: Madison, WI, 1998.
(33) Reed, A. E.; Curtiss, L. A.; Weinhold, F. *Chem. Rev.* **1988**, *88*, 899−926.
(34) Weinhold, F.; Carpenter, J. E. In *The Structure of Small Molecules and Ions*; Naaman, R., Vager, Z., Eds. Plenum: New York, 1988; pp 227−236.
(35) Peralta, J. E.; Contreras, R. H.; Snyder, J. P. *Chem. Commun.* **2000**, 2025−2026.

matrix, ϕ_i is the ith atomic orbital, and $\delta(r_N)$ is the Dirac delta function centered at the position of nucleus N. Equation 3 is an expression that can be evaluated by simply computing the product of the amplitudes of atomic orbitals ϕ_i and ϕ_j at the position of nucleus N.

The finite perturbation method employed for computing scalar couplings involves adding a Fermi contact perturbation of the form $\lambda\langle\phi_i|\delta(r_M)|\phi_j\rangle$ (where λ is the perturbation parameter) to the ijth element of the α-spin H_0 matrix and subtracting the perturbation from the corresponding element of the β-spin H_0 matrix. This results in the production of unpaired electron spin density Δ, which propagates throughout the molecule as self-consistency is achieved. Finally, the Fermi contact portion of the coupling can be computed using finite difference methods

$$J_{MN} = \left(\frac{\hbar}{2\pi}\right)\left(\frac{8\pi\mu_b}{3}\right)^2 \gamma_M\gamma_N\lambda^{-1}\Delta \tag{4}$$

where γ_M and γ_N are the gyromagnetic ratios for nuclei M and N, respectively. Despite the fact that this method perturbs the wave function in such a way as to yield powerful information about *J*-coupling, the perturbed wave function is still nearly indistinguishable from the closed shell, unperturbed wave function.

Equation 3 can be easily modified so that the Fermi contact spin density is computed in terms of NLMOs

$$\Delta = \sum_i \Gamma_{ii}[\langle\Omega_i^\alpha|\delta(r_N)|\Omega_i^\alpha\rangle - \langle\Omega_i^\beta|\delta(r_N)|\Omega_i^\beta\rangle] \tag{5}$$

where Ω_i^α and Ω_i^β are the ith α- and β-spin NLMOs, and r_N is the coordinate of the atom where the spin density is being observed. By switching to the NLMO basis, the double sum in eq 3 can be reduced to a single sum, because Γ is diagonal in the NLMO basis. It should also be noted that the NLMO contributions computed from eq 5 are at the level of detail obtained from previously published NBO-based analyses of *J*-couplings.[35]

The NLMOs in eq 5 can be broken down further into a linear combination of NBOs

$$\Omega_i(\vec{r}) = \sum_j c_{ji}\sigma_j(\vec{r}) \tag{6}$$

Each NLMO Ω_i in eq 5 contains a large contribution ($c_{ii} \cong 1$) from a parent Lewis NBO σ_i and smaller contributions from non-Lewis NBOs σ_j* into which σ_i delocalizes by conjugative or hyperconjugative interactions. Thus, we can picture each term in eq 5 as having a "Lewis" (localized) contribution $\Delta_i^{(L)}$ from the NBO σ_i and a residual "non-Lewis" (delocalized) contribution $\Delta_i^{(NL)}$ from all remaining non-Lewis NBOs σ_j*

$$\Delta = \sum_i^{occ}[\Delta_i^{(L)} + \Delta_i^{(NL)}] \tag{7}$$

The contribution $\Delta_i^{(L)}$ corresponds to a strictly localized "natural Lewis structure" determinantal wave function of doubly occupied Lewis NBOs (i.e., $\Omega_i = \sigma_i$) and can be evaluated as

$$\Delta_i^{(L)} = \langle\sigma_i^\alpha|\delta(r_N)|\sigma_i^\alpha\rangle - \langle\sigma_i^\beta|\delta(r_N)|\sigma_i^\beta\rangle \tag{8}$$

The $\Delta_i^{(NL)}$ term is evaluated by difference as

$$\Delta_i^{(NL)} = \Delta_i - \Delta_i^{(L)} \tag{9}$$

using the ith NLMO contribution (Δ_i) in eq 5. Further details are given in the Appendix.

The non-Lewis contribution ($\Delta_i^{(NL)}$) in eq 9 is further separated into two components

$$\Delta_i^{(NL)} = \Delta_i^{(deloc)} + \Delta_i^{(repol)} \tag{10}$$

In each case, the subscript i denotes the parent Lewis-type NBO (σ_i) with which this is associated. The "deloc" superscript is used to designate the portion of the non-Lewis contribution resulting from *delocalization* ("resonance") effects of conjugative or hyperconjugative type. As the name implies, such "delocalization" involves transfer of electron density from parent NBO σ_i into a non-Lewis orbital (antibond σ_j* or Rydberg-type ry_j*) centered in some *different* region of the molecule. In contrast, the "repol" superscript denotes the *residual repolarization* contribution that results when electron density from σ_i is transferred into valence antibond σ_i* or Rydberg-type ry_i* in the *same* bonding region. The $\Delta_i^{(repol)}$ contribution therefore corresponds to *intra*bond redistribution of electron density *within* the region of parent σ_i, merely "repolarizing" the σ_i bond but not altering the basic Lewis structure pattern. $\Delta_i^{(repol)}$ can be considered as a type of "electron correlation" correction to σ_i (as described below), closely related to the parent Lewis contribution $\Delta_i^{(L)}$ which it modifies. The $\Delta_i^{(L)}$, $\Delta_i^{(repol)}$ "parent" entries are therefore grouped together at the top of NJC output table (cf., Table 1), followed by the individual and total $\Delta_i^{(deloc)}$ entries.

The delocalization contribution for each Ω_i can be decomposed, in turn, into contributions from each non-Lewis NBO σ_j*

$$\Delta_i^{(deloc)} = \sum_j^{NL}\Delta_{i\rightarrow j^*}^{(deloc)} \tag{11}$$

where $\Delta_{i\rightarrow j^*}^{(deloc)}$ is the contribution associated with $\sigma_i \rightarrow \sigma_j$* delocalization. The dissection of *J*-coupling into Lewis and non-Lewis NBO contributions follows the pattern that has been found useful for many other properties.[32] In this way, the coupling can be partitioned into contributions of three distinct varieties

$$J = J^{(L)} + J^{(deloc)} + J^{(repol)} \tag{12}$$

The terms in the NBO expansion are expected to obey a few simple principles. First, in a localized basis, only orbitals near the coupled atoms are likely to have significant amplitude at those nuclear centers. Thus, despite the possibility that orbitals distant to the coupled nuclei may respond strongly to the perturbation, remote orbitals are unlikely to play a significant role in the coupling mechanism, owing to their negligible amplitude at the positions of the coupled nuclei. Orbitals with high s-character centered on the coupled nuclei (e.g., σ and σ* orbitals) are those most likely to make large contributions to *J*-coupling, because they have the greatest amplitude at the coupled nuclei. Finally, the same types of NBO interactions that contribute to hyperconjugative delocalization or steric effects for other properties are also likely to be involved in the corresponding contributions for scalar coupling: $J^{(deloc)}$ and $J^{(L)}$.

1. Lewis Coupling Contribution, $J^{(L)}$. As stated above, the Lewis contribution ($\Delta^{(L)}$) refers to the spin density that results from the slight shift in the natural Lewis structures of the α- and β-spin orbitals in response to the perturbation. The Lewis contribution can work with or against the delocalization spin density, depending on the chemical environment of the molecule (i.e., it can have the same or opposite sign as the delocalization contribution(s)). Because nearly all of the electron density is

contained within the natural Lewis structure, it is not surprising that the $\Delta^{(L)}$ contribution accounts for the majority of the coupling in most systems (about 70% of J_{HH} coupling in aliphatic compounds).

Spin information can be communicated between electrons in distinct bond pairs by means of the *exchange antisymmetry* property of the wave function. This is essentially the origin of *steric* effects, which arise from the fact that electrons in one bond region cannot be perturbed in a way that violates the Pauli principle in any other region. Spin perturbations in NBO σ_i are therefore accompanied by Pauli-preserving adjustments in other filled NBO σ_j, no matter how localized the NBOs. Weisskopf has shown that such steric effects can be pictured vividly in terms of "kinetic energy pressure", associated with the requirement that orbitals maintain mutual *orthogonality* to ensure compliance with the Pauli principle.[36] (Palke and co-workers have also demonstrated that "exchange effects" are primarily attributable to the implicit orthogonalization of orbitals in a Slater determinant.)[37,38] When orbitals σ_i, σ_j are crowded into the same spatial region, they necessarily develop "orthogonalization tails" (i.e., small oscillatory nodal features that increase the curvature and kinetic energy) to avoid the impending overlap and violation of the Pauli principle. Thus, a perturbation in σ_i that distorts the spatial distribution of α- or β-spin requires compensating changes in σ_j to maintain mutual orthogonality. These highly interconnected orthogonalization features can readily be seen in the forms of the NBOs discussed here, even for cases where σ_i, σ_j are separated spatially by several chemical bonds.

Because spin transfer by means of steric exchange orthogonalization is not dependent on conjugative or hyperconjugative delocalization pathways, it resembles a "through-space" interaction in that the bonds involved do not follow a donor−acceptor style spin transfer. In addition, the steric mechanism is oftentimes counterintuitive, because the amplitudes of atomic orbitals decrease exponentially with distance, which would apparently preclude the possibility of having appreciable amplitude at the position of an atom even a few bonds away. However, the extreme sensitivity of the Fermi contact operator to such nodal features causes the orthogonalization tails to be an important means for transferring spin density. This feature typically makes steric exchange the dominant mechanism of spin coupling, even when strong hyperconjugative delocalization is present.

2. Interbond Spin Delocalization Contribution, $J^{(deloc)}$. The interbond delocalization mechanism is a means for transferring spin density between bonding regions by means of donor−acceptor interactions that are either conjugative ($\pi-\pi^*$) or hyperconjugative ($\pi-\sigma^*$, $\sigma-\pi^*$, $\sigma-\sigma^*$). As mentioned above, only σ, σ^* orbitals on the coupled nuclei make appreciable contributions to *J*-coupling, so hyperconjugative phenomena are typically far more important than conjugative phenomena. The pathways available for the transfer of spin density are often the same as those involved in stabilizing (energy lowering) interactions. Thus, when present, the hyperconjugative delocalization mechanism commonly yields spin coupling patterns that are consistent with stereoelectronic phenomena.

While the number of bonding (σ) and antibonding (σ^*) orbitals depends only on the size of the valence shell, and is thus independent of the total number of basis functions, the number of single-center Rydberg (ry^*) orbitals grows rapidly with basis extension. To preserve focus on the valence orbitals, which contribute most strongly to spin coupling, the delocalization contributions corresponding to all ry^* on a given center are accumulated into a single contribution for each NMLO in the NJC output (see in a later section).

3. Residual Intrabond Repolarization Contribution, $J^{(repol)}$. As mentioned above, the $J^{(repol)}$ contribution corresponds to repolarization of electron density within the parent σ_i bond region and, as such, represents intrabond "reorganization" within the same overall Lewis pattern. The primary contributor to $J^{(repol)}$ is the interaction of σ_i with its *own* antibond ($\sigma_i \rightarrow \sigma_i^*$). Suppose that σ_i, σ_i^* correspond to the A−B bond region, with

$$\sigma_{AB} = c_A h_A + c_B h_B \tag{13}$$

$$\sigma^*_{AB} = c_B h_A - c_A h_B \tag{14}$$

The unitary mixing of σ_{AB}, σ_{AB}^* (with mixing coefficient *f*) merely results in a repolarized A−B bond orbital $\tilde{\sigma}_{AB}$

$$\tilde{\sigma}_{AB} = (1-f^2)^{-1/2}\sigma_{AB} + f\sigma^*_{AB} = \tilde{c}_A h_A + \tilde{c}_B h_B \tag{15}$$

with modified polarization coefficients

$$\tilde{c}_A = (1-f^2)^{-1/2} c_A + \lambda c_B \tag{16}$$

$$\tilde{c}_B = (1-f^2)^{-1/2} c_B - \lambda c_A \tag{17}$$

Such mixings are normally absent in uncorrelated spin-free wave functions, because the original polarization coefficients c_A, c_B are already the *best possible* to describe the electron density. However, such mixings may occur in *correlated* wave functions to achieve the expected "different orbitals for different spins" description of a correlated electron pair (e.g., differential left−right polarization of α- and β-spin orbitals to incorporate left−right correlation). From this viewpoint, the $\sigma_{AB} \rightarrow ry_A^*$, ry_B^* repolarizations correspond to radial (in−out) or angular (up−down) correlations, while the $\sigma_{AB} \rightarrow \sigma^*_{AB}$ repolarization corresponds to bond (left−right) correlation. Electron correlation is therefore a powerful "mechanism" for differential distribution of α- and β-electron spin density, that is, for creation of nonzero spin density throughout the bond region. Even if such repolarizations (correlations) are absent in the field-free limit, the Fermi spin perturbation can create nonzero "correlations" of this type that contribute to $J^{(repol)}$. Although the $J^{(repol)}$ contributions usually appear to be fairly insignificant compared to $J^{(L)}$ and $J^{(deloc)}$, they represent a distinct "type" of *J*-coupling mechanism that may become important in highly correlated systems.

III. Methods

Calculations were performed with the Gaussian 98[39] electronic structure program. The (hybrid) density functional B3LYP[40] was used for all calculations. In addition, the 6-311G** basis was used unless otherwise noted. All coupling calculations were performed using a

(36) Weisskopf, V. F. *Science* **1975**, *187*, 605−612.
(37) Christiansen, P. A.; Palke, W. E. *Chem. Phys. Lett.* **1975**, *31*, 462−466.
(38) Christiansen, P. A.; Palke, W. E. *J. Chem. Phys.* **1977**, *67*, 57−63.
(39) Frisch, M. J.; Trucks, G. W.; Schlegel, G. E.; Scuseria, G. E.; Robb, M. A.; Cheeseman, J. R.; Zakrzewski, V. G.; Montgomery, J. A., Jr.; Stratmann, R. E.; Burant, J. C.; Dapprich, S.; Millam, J. M.; Daniels, A. D.; Kudin, K. N.; Strain, M. C.; Farkas, O.; Tomasi, J.; Barone, V.; Cossi, M.; Cammi, R.; Mennucci, B.; Pomelli, C.; Adamo, C.; Clifford, S.; Ochtershki, J.; Petersson, G. A.; Ayala, P. Y.; Cui, Q.; Morokuma, K.; Malick, D. K.; Rabuck, A. D.; Raghavachari, K.; Foresman, J. B.; Cioslowski, J.; Ortiz, J. V.; Baboul, A. G.; Stefanov, B. B.; Liu, G.; Liashenko, A.; Piskorz, P.; Komaromi, I.; Gomperts, R.; Martin, R. L.; Fox, D. J.; Keith, T.; Al-Laham, M. A.; Peng, C. Y.; Nanayakkara, A.; Challacombe, M.; Gill, P. M. W.; Johnson, B.; Chen, W.; Wong, M. W.; Andres, J. L.; Gonzalez, C.; Head-Gordon, M.; Replogle, E. S.; Pople, J. A. *Gaussian 98*, revision A.9; Gaussian, Inc.: Pittsburgh, PA, 1998.
(40) Becke, A. D. *J. Chem. Phys.* **1993**, *98*, 5648−5652.

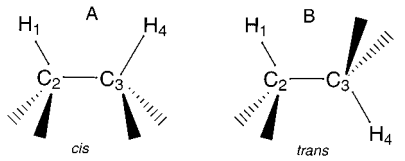

Figure 1. Ethane model: A. cis conformation with 0° torsion angle and B. trans conformation with 180° torsion angle.

Fermi contact perturbation of 0.02 au. The field strength was chosen so that there is no residual dependence on the calculated *J*-values (within the specified 0.01 Hz precision) on the λ parameter. Molecular structures were first fully optimized at B3LYP/6-311G** and then modified as discussed. Structural diagrams were made with ChemDraw Pro (CambridgeSoft, Cambridge, MA), graphs were made using Sigma Plot 2000 (SPSS, Chicago, IL), and two-dimensional orbital contour plots were made with Orbplot (Theoretical Chemistry Institute, University of Wisconsin, Madison, see the NBO 5.0 website[41]). NJC is implemented in NBO version 5.0.[41]

IV. Results and Discussion

1. $^3J_{HH}$ Vicinal Coupling in Ethane. We first use ethane to illustrate the kind of results that can be obtained from NJC analysis. Ethane is a useful model because of its role as a prototype for vicinal *J*-coupling in a broad range of organic and biological molecules.[2,3] In addition, substantial experimental evidence suggests that numerous heteronuclear ^3J couplings exhibit Karplus-like dependence.[13]

Table 1 shows a summary of the main NBO contributions (in a form that approximates the output of the NJC program) for trans $^3J_{HH}$ vicinal couplings in the ethane model rotamer shown in Figure 1B. The net calculated $^3J_{HH}$ coupling is 14.72 Hz for trans ethane. The average of the calculated couplings for the 60°, 120°, and 180° positions (staggered ethane) is 7.4 Hz, which is close to the experimentally measured value of about 8 Hz. Residual discrepancies may be due to neglect of vibrational motions, second-order correlation in the Fermi-Contact term, or residual non-Fermi contact contributions as have been discussed by others.[42−44]

The total Lewis contribution of +10.97 Hz shown in Table 1 represents about 75% of the total coupling of +14.72 Hz. This is in agreement with the generalization that approximately 70% of the coupling is accounted for by the natural Lewis structure in alkane couplings. Such a large Lewis contribution is not surprising, given that 99.98% or more of the electron density resides in the formal Lewis structure described by the set of Lewis-type NBOs. The first row in Table 1 summarizes the leading terms in the Lewis contribution.

The $J^{(L)}$ components of the σ_{C2H1} and σ_{C3H4} NLMOs each provide +5.52 Hz. Their contributions are identical because of the high symmetry in the trans ethane molecule. For simplicity, the sum of the Lewis contributions from σ_{C2H1} and σ_{C3H4} will be referred to as $J_{vic}^{(L)}$ to emphasize their vicinal relationship. From Table 1, it is apparent that the $J_{vic}^{(L)}$ contribution accounts for all but −0.06 Hz of the total 10.97 Hz from the natural Lewis structure. This result is also consistent with chemical intuition, because it is expected that the σ_{C2H1} and σ_{C3H4} bonds would be the electron pairs most relevant to the coupled nuclei H_1 and H_4.

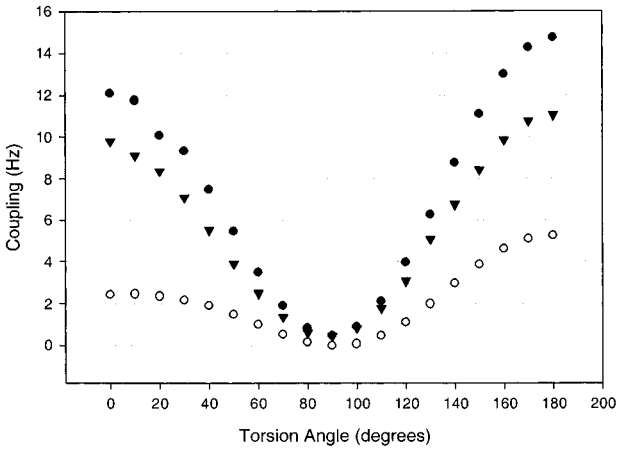

Figure 2. Calculated coupling, $J_{vic}^{(L)}$, and $J_{vic}^{(deloc)}$ terms for ethane plotted as a function of torsion angle. The trans ground state was taken as the starting geometry, and each other torsion angle was the result of a rigid rotation about the C_2-C_3 bond. The C_2-C_3 bond length was optimized at each torsion angle before the coupling calculation was performed. Symbol definitions: net coupling corresponds to filled circles (●), $J_{vic}^{(deloc)}$ is given by open circles (○), and $J_{vic}^{(L)}$ is shown as triangles (▼).

The remaining large contributions to H_1-H_4 coupling arise from the three-bond vicinal $\sigma_{C2H1} \rightarrow \sigma_{C3H4}^*$ and $\sigma_{C3H4} \rightarrow \sigma_{C2H1}^*$ delocalization interactions (each accounting for 2.63 Hz, as shown in Table 1). The sum of these two contributions will be referred to as $J_{vic}^{(deloc)}$. Each of the remaining delocalization contributions is smaller than the threshold (1.0 Hz) for listing as a separate row in Table 1; the sum of these appears in the row entitled "others". The subtotal of $J^{(deloc)}$ for each NLMO is given in parentheses (i.e., 1.58 Hz for the σ_{C2H1} and σ_{C3H4} NLMOs). Finally, the addition of the −0.07 Hz residual repolarization contribution yields a total contribution of 7.02 Hz from each of the σ_{C2H1} and σ_{C3H4} NLMOs; their sum accounts for all but 0.68 Hz of the total 14.72 Hz coupling. Table 1 illustrates how the coupling contributions can be treated in a compact and complete manner in terms of a very small number of NBO interactions.

The Karplus curve shown in Figure 2 displays how the net couplings, as well as the $J_{vic}^{(L)}$ and $J_{vic}^{(deloc)}$ contributions, vary with rotation about the C_2-C_3 bond. From the plot, it can be seen that both $J_{vic}^{(L)}$ and $J_{vic}^{(deloc)}$ contribute to the strong dihedral dependence over the 180° range. In addition, the sum of the $J_{vic}^{(L)}$ and $J_{vic}^{(deloc)}$ contributions accounts for nearly all the net coupling over the entire angular range. This strong mutual dependence on geometry is further demonstrated in Figure 3, where the C_2-C_3 bond distance for the trans ethane model varied about the equilibrium distance of about 1.5 Å (shown in Figure 1B). As expected, the net couplings, $J_{vic}^{(L)}$and $J_{vic}^{(deloc)}$, decrease exponentially as the C_2-C_3 bond distance increases. The plots in Figures 2 and 3 are designed to isolate the interactions between the σ_{C2H1} and σ_{C3H4} NBOs and their associated antibonding σ^* NBOs, while holding the orbital forms (i.e., hybridization, polarization, etc.) relatively constant. The nature of the interactions is discussed in detail in the following sections.

A. Steric Exchange Antisymmetry and $J_{vic}^{(L)}$ in Ethane Vicinal Coupling. As stated in the Theory section, the $J^{(L)}$ contribution is closely related to the concept of steric exchange

(41) Glendening, E. D.; Badenhoop, J. K.; Reed, A. E.; Carpenter, J. E.; Bohmann, J. A.; Morales, C. M.; Weinhold, F. *NBO 5.0*; Theoretical Chemistry Institute, University of Wisconsin: Madison, WI, 2001.

(42) Fukui, H.; Inomata, H.; Baba, T.; Miura, K.; Matsuda, H. *J. Chem. Phys.* **1995**, *103*, 6597−6600.

(43) Malkina, O. L.; Salahub, D. R.; Malkin, V. G. *J. Chem. Phys.* **1996**, *105*, 8793−8800.

(44) Helgaker, T.; Jaszunski, M.; Ruud, K. *Chem. Rev.* **1999**, *99*, 293−352.

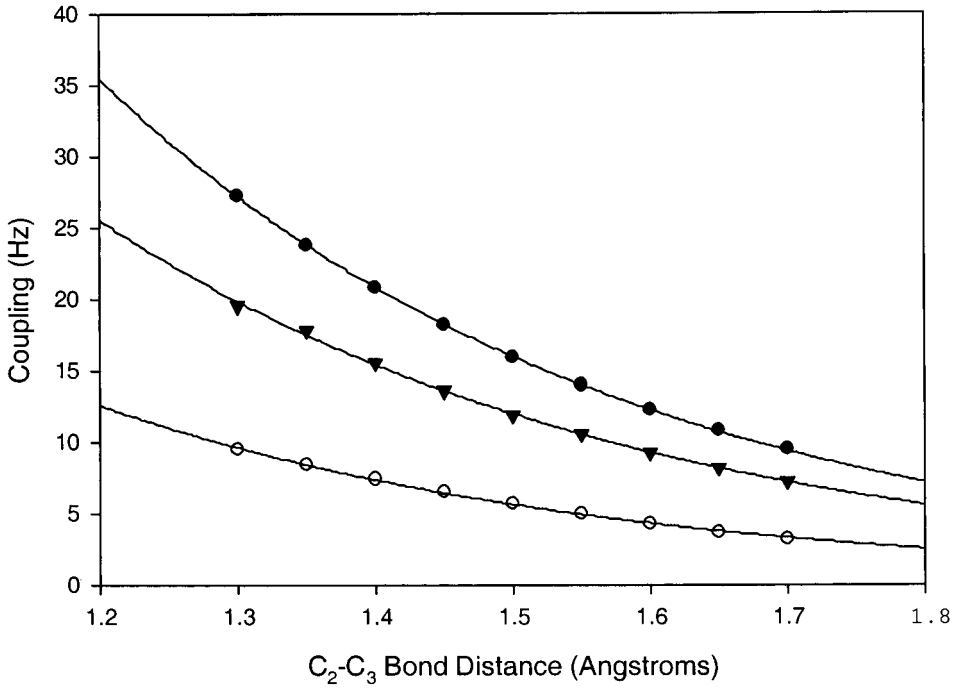

Figure 3. Calculated coupling in trans ethane, $J_{vic}^{(L)}$, and $J_{vic}^{(deloc)}$ plotted as a function of the C_2-C_3. The three curves were fitted with single-exponential decay functions (that go to zero at infinite distance), with an R^2 of 0.99 or better for each. Symbol definitions: net coupling corresponds to filled circles (●), $J_{vic}^{(deloc)}$ is given by open circles (○), and $J_{vic}^{(L)}$ is shown as triangles (▼).

antisymmetry. That is, the motion of same-spin electrons is correlated as a consequence of Pauli exclusion. As a result, a perturbation in the spatial distribution of a spin orbital is followed by Pauli-preserving responses from the rest of the orbitals in order to maintain mutual orthogonality. In this way, such steric interactions can provide a method of propagating spin density throughout a molecule, because the α- and β-spin NBOs can respond differently to the perturbation. For example, in the case of the trans ethane model, a spin perturbation at H_1 can be communicated to H_4 by steric contact between the α- and β-spin σ_{C2H1} and σ_{C3H4} NBOs. In other words, an adjustment in the spatial distribution of the α-spin σ_{C2H1} NBO in response to the spin perturbation at H_1 requires that the α-spin σ_{C3H4} NBO also be adjusted to maintain orthogonality. The same is true for the β-spin σ_{C2H1} and σ_{C3H4} NBOs. Because the α- and β-spin σ_{C3H4} NBOs respond independently to the perturbation, unquenched electron spin angular momentum at H_4 (i.e., Fermi contact spin density) can result, thus propagating the coupling.

The relationship between the steric contact of the σ_{C2H1} and σ_{C3H4} spin NBOs can be tested by correlating the pairwise steric energy between the σ_{C2H1} and σ_{C3H4} NBOs with $J_{vic}^{(L)}$. Although the total exchange energy of a system involves N electrons simultaneously, the pairwise steric energy E^x between two NBOs, σ_i and σ_j, can be accurately approximated by

$$E_{ij}^{x} = (F_{ii}^{NBO} - F_{ii}^{PNBO/2}) + (F_{jj}^{NBO} - F_{jj}^{PNBO/2}) \qquad (18)$$

where the "PNBO/2" orbital is formed by deorthogonalizing only NBOs i,j in a reverse Löwdin transformation, and F_{ii} denotes the iith Fock matrix element in the NBO and PNBO/2 basis sets.[45,46] Figure 4 shows $J_{vic}^{(L)}$ plotted as a function of the pairwise steric exchange energy between σ_{C2H1} and σ_{C3H4} NBOs for each torsion angle in the Karplus curve shown in Figure 2. Figure 5 shows $J_{vic}^{(L)}$ plotted as a function of the pairwise steric energy for each C_2-C_3 bond distance point from Figure 3. Figures 4 and 5 display the strong linear correlation between

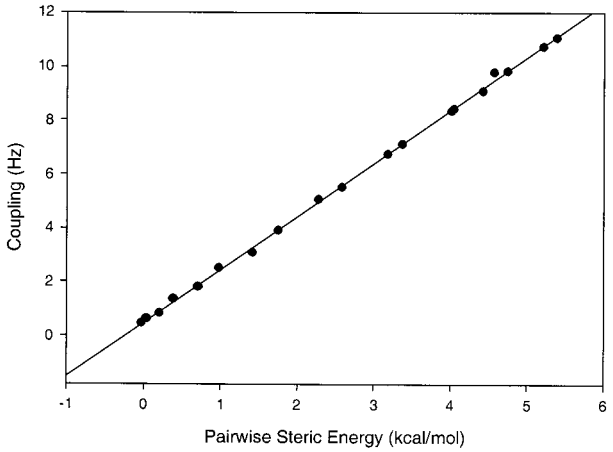

Figure 4. Calculated $J_{vic}^{(L)}$ versus the pairwise steric energy between the σ_{C2H1} and σ_{C3H4} NBOs at each torsion angle from 0° to 180° of the Karplus curve shown in Figure 2. $J_{vic}^{(L)}$ is shown by filled circles (●).

the pairwise steric energy and $J_{vic}^{(L)}$. Essentially, this result suggests that the degree to which the α- and β-spin forms of the σ_{C2H1} and σ_{C3H4} NBOs differ is strongly related to their steric contact. This is in accord with the physical picture inferred by Barfield and Karplus, where coupling was computed using valence bond 2nd order perturbation theory analysis.[47,48] Although the underlying physical model of Barfield and Karplus is quite different from that of the finite perturbation method, many of their conclusions can be readily mapped onto concepts presented in this paper. In particular, their analysis of Penney−Dirac bond orders, which are further expressed in terms of

(45) Badenhoop, J. K.; Weinhold, F. *J. Chem. Phys.* **1997**, *107*, 5406−5421.
(46) Badenhoop, J. K.; Weinhold, F. *J. Chem. Phys.* **1997**, *107*, 5422−5432.
(47) Barfield, M.; Karplus, M. *J. Am. Chem. Soc.* **1969**, *91*, 1−10.
(48) Barfield, M.; Chakrabarti, B. *Chem. Rev.* **1969**, *69*, 757−777.

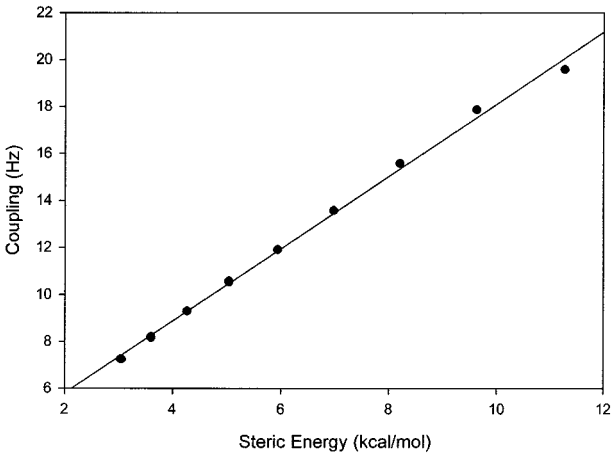

Figure 5. Plot of $J_{vic}^{(L)}$ versus the pairwise steric energy between the σ_{C2H1} and σ_{C3H4} NBOs at each C_2-C_3 bond distance point from 1.3 to 1.7 Å shown in Figure 3. $J_{vic}^{(L)}$ is shown as filled circles (●).

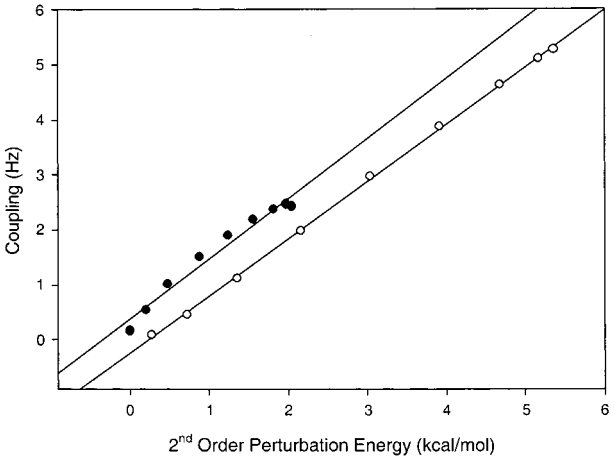

Figure 6. Calculated $J_{vic}^{(deloc)}$ versus the sum of the 2nd order perturbation energies associated with the $\sigma_{C2H1} \rightarrow \sigma_{C3H4}^*$ and $\sigma_{C3H4} \rightarrow \sigma_{C2H1}^*$ vicinal delocalizations for each torsion angle from 0° to 180° of the Karplus curve shown in Figure 2. Symbol definitions: $J_{vic}^{(deloc)}$ from 0° to 80° corresponds to filled circles (●), and $J_{vic}^{(deloc)}$ from 100° to 180° is given by open circles (○).

formal, two-electron valence bond exchange integrals, are related to the steric mechanism presented here. Furthermore, their "direct" coupling mechanism is analogous to our *steric* coupling mechanism, and their "indirect" coupling mechanism is related to our *delocalization* coupling mechanism.

B. Vicinal $\sigma \rightarrow \sigma^*$ Delocalization and $J_{vic}^{(deloc)}$ in Ethane $^3J_{HH}$ Coupling. As with the steric contribution $J_{vic}^{(L)}$, $J_{vic}^{(deloc)}$ can be related to energetic changes associated specifically with delocalization. Whereas $J_{vic}^{(L)}$ corresponds to *destabilizing* (repulsive) steric-type interactions, $J_{vic}^{(deloc)}$ corresponds to the *stabilizing* energy associated with the $\sigma_{C2H1} \rightarrow \sigma_{C3H4}^*$ and $\sigma_{C3H4} \rightarrow \sigma_{C2H1}^*$ hyperconjugative electron delocalization pathways. The energy associated with these delocalizations can be approximated accurately by 2nd order perturbation theory

$$E_{i \rightarrow j}^{(2)} = -2\frac{\langle \sigma_i | \hat{F} | \sigma_j^* \rangle^2}{\epsilon_{\sigma_j^*} - \epsilon_{\sigma_i}} \qquad (19)$$

where ϵ_{σ_i} is the energy of NBO σ_i (i.e., $\epsilon_{\sigma_i} = \langle \sigma_i | \hat{F} | \sigma_i \rangle$). Similar to steric energy, the 2nd order perturbation energy is also a measure of the "contact" between orbitals. Figure 6 shows

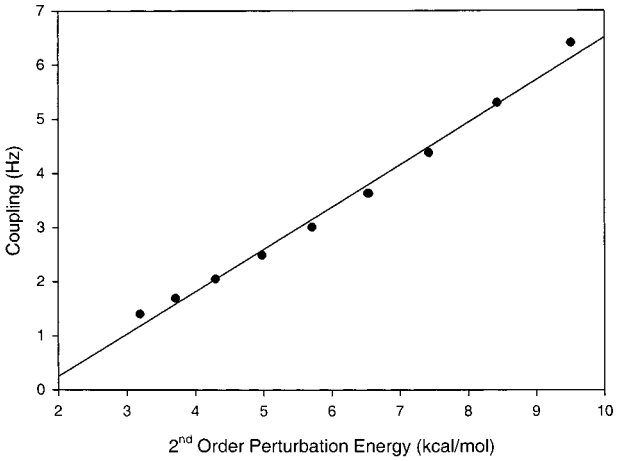

Figure 7. Calculated $J_{vic}^{(deloc)}$ plotted as a function of the sum of the 2nd order perturbation energies associated with the $\sigma_{C2H1} \rightarrow \sigma_{C3H4}^*$ and $\sigma_{C3H4} \rightarrow \sigma_{C2H1}^*$ vicinal delocalizations each for each C_2-C_3 bond distance point from 1.3 to 1.7 Å in Figure 3. $J_{vic}^{(deloc)}$ is shown as filled circles (●).

$J_{vic}^{(deloc)}$ plotted as a function of the 2nd order perturbation energy associated with the $\sigma_{C2H1} \rightarrow \sigma_{C3H4}^*$ and $\sigma_{C3H4} \rightarrow \sigma_{C2H1}^*$ hyperconjugative delocalizations for each torsion angle in the Karplus curve shown in Figure 2. Separate fits were made for torsion angles from 0° to 80° and from 100° to 180°, because different slopes and intercepts were found for each angular region. This discrepancy likely arises from differing nodal features presented to the donor σ NBO for angles greater than and less than 90°. Although the slope and intercept for $J_{vic}^{(deloc)}$ are greater for angles > 90°, the coupling contributions are lower in this angular region, because the energy associated with the $J_{vic}^{(deloc)}$ delocalization mechanism is lower. Figure 7 displays $J_{vic}^{(deloc)}$ plotted as a function of the 2nd order energy for each of the C_2-C_3 bond distance points in Figure 3. Both Figures 6 and 7 illustrate the strong linear relationship that exists between $J_{vic}^{(deloc)}$ and the energies of the $\sigma_{C2H1} \rightarrow \sigma_{C3H4}^*$ and $\sigma_{C3H4} \rightarrow \sigma_{C2H1}^*$ hyperconjugative delocalizations, which again displays how coupling can be propagated by pairwise NBO interactions of distinguishable physical type.

C. Role of Orbital Overlap in Determining $J_{vic}^{(L)}$ and $J_{vic}^{(deloc)}$. Because chemists are used to thinking of molecular electronic structure interactions in terms of orbital overlaps, it is conceptually useful to be able to view underlying *J*-coupling contributions in terms of orbital overlap. However, NBOs form an orthonormal basis, and are thus unable to provide such a picture. Instead, the pre-NBOs (PNBOs), the nonorthogonal precursors of the NBOs, are more suitable because they lack the final interatomic orthogonalization step of the NBOs. As a result, the PNBOs provide a convenient way in which to view orbital interactions. Each PNBO remains orthogonal to the PNBOs on the same center but has nonvanishing overlap with those on other atoms. In accordance with a Mulliken-type approximation, the corresponding Hamiltonian interaction elements are found to be closely proportional to these overlap integrals

$$\langle \sigma_A^{NBO} | \hat{F} | \sigma_B^{NBO} \rangle \propto \langle \sigma_A^{PNBO} | \sigma_B^{PNBO} \rangle \qquad (20)$$

Therefore, the interatomic steric and delocalization energies (and corresponding $J_{vic}^{(L)}$ and $J_{vic}^{(deloc)}$ coupling contributions) can be related to their PNBO overlaps. To illustrate this, the $J_{vic}^{(L)}$

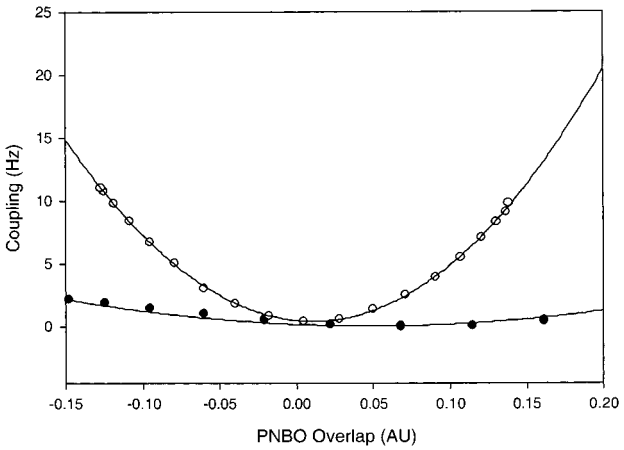

Figure 8. Calculated $J_{vic}^{(deloc)}$ and $J_{vic}^{(L)}$ plotted as a function of their corresponding PNBO overlaps at each torsion angle from 0° to 180°. The largest negative overlap for $J_{vic}^{(deloc)}$ and the largest positive overlap for $J_{vic}^{(L)}$ correspond to a torsion angle of 0°. The largest positive overlap for $J_{vic}^{(deloc)}$ and the largest negative overlap for $J_{vic}^{(L)}$ correspond to a torsion angle of 180°. Symbol definitions: $J_{vic}^{(deloc)}$ corresponds to filled circles (●), and $J_{vic}^{(L)}$ is given by open circles (○).

and $J_{vic}^{(deloc)}$ contributions are plotted in Figure 8 as a function of their respective PNBO overlaps, $S_{\sigma\sigma}$ and $S_{\sigma\sigma}$*.

The $J_{vic}^{(deloc)}$ contribution can be conceptualized in a straightforward way as resulting from the donation of coupling (spin density) from a high-occupancy Lewis NBO σ_i into a low-occupancy antibonding NBO σ_j*. This donor−acceptor interaction can be related to a simple overlap between the orbitals involved. From Figure 8, it appears that both $J_{vic}^{(deloc)}$ and $J_{vic}^{(L)}$ vary quadratically with respect to their PNBO overlaps. However, $J_{vic}^{(L)}$ has greater curvature, indicating that the steric (filled−filled) orbital interaction is *more* responsive to the changing overlap of σ_{C2H1} and σ_{C3H4} than the hyperconjugative delocalization interaction, $J_{vic}^{(deloc)}$. This is evidently due to the fact that the $J_{vic}^{(L)}$ contribution involves two high occupancy NBOs. Figure 9 shows two-dimensional contour plots of the $\sigma_{C2H1} - \sigma_{C3H4}$ and $\sigma_{C2H1} - \sigma_{C3H4}$* PNBO overlaps for cis (Figures 9A and 9B) and trans (Figures 9C and 9D) conformers. By comparing the $\sigma_{C2H1} - \sigma_{C3H4}$* PNBO overlaps in Figures 9B and 9D, it is apparent that the trans PNBO overlap (9D) is more favorable than the cis (9B), which accounts for the conformational preference and associated C−C shortening.[49] The shorter C_2-C_3 bond distance in the trans rotamer, corresponding to greater overlap (and steric coupling contribution) between the $\sigma_{C2H1} - \sigma_{C3H4}$ bonds, leads to an accompanying strong contribution of $J_{vic}^{(L)}$ to spin coupling. Thus, although steric effects are *secondary* to hyperconjugative effects in the *energetics* of conformational change, the relative importance of "steric" versus "hyperconjugative" contributions is *reversed* in *J*-coupling, because *filled* σ orbitals carry a much stronger Fermi contact amplitude at the nuclei than low-occupancy σ* NBOs.

D. Basis Set Dependence of Scalar Coupling Contributions. Because the Fermi contact spin density is determined only by the form of the wave function at a single point in space (i.e., the nuclear position of an atom in the coupling pair), it is expected to be exquisitely sensitive to the quality of the basis set, especially at the cusp of the s-type atomic orbital basis functions. With this in mind, it is interesting to ask how the coupling contributions are affected as the basis set expands. As stated above, when basis functions are added, the number of filled Lewis-like orbitals (e.g., σ NBOs) and valence antibonding orbitals (e.g., σ* NBOs) remains constant, while the number of Rydberg orbitals increases. As a result, the number of available acceptor orbitals increases as the size of the basis increases. To demonstrate the effect of increasing the size of the basis, a summary of the basis set dependence on the net and individual coupling contributions is shown in Table 2. The types of basis sets used range from Pople-style (6-31+G*, 6-311G**, and 6-311++G**) to Dunning-type correlation consistent sets (cc-pVDZ, cc-pVTZ, and aug-cc-pVDZ), in addition to full double-ζ for increased core flexibility (D95). From Table 2, it is apparent that, in all cases, the sum of $J_{vic}^{(L)}$ and $J_{vic}^{(deloc)}$ for each basis listed is always greater than the net coupling by about 12−20%. This requires that the sum of the remaining small contributions (in the row labeled "others") be negative. In addition, the $J_{vic}^{(deloc)}$ contribution is roughly 50% of the $J_{vic}^{(L)}$ contribution over all basis sets. However, no clear correlations were observed between the net coupling and basis size and individual coupling contributions.

The fact that the NBO contributions are roughly consistent over all basis sets is a consequence of their design. In particular, the set of NBOs is occupancy-ordered to condense maximum electron density into the leading (valence-type) NBOs, and residual Rydberg orbitals (even though more numerous) do *not* gain appreciable significance as the basis expands.[33] In other words, despite the fact that NJC does not contain predetermined biases toward producing a small number of constituent coupling contributions, this result can be expected over a wide range of molecular models as a result of the underlying method of NBO construction.

2. $^6J_{HH}$ Coupling in *n*-Pentane. Pentane (Figure 10A) provides an excellent model for describing long-range coupling. In comparison to ethane, the steric exchange mechanism is expected to become relatively more important in the long-range $^6J_{HH}$ coupling of pentane, because the coupled protons are not connected by the strong hyperconjugative delocalization pathways typically found in shorter range coupling pairs (e.g., $^3J_{HH}$ vicinal coupling). Table 3 lists the coupling contributions to $^6J_{HH}$ by basis set; these contributions are abbreviated as $J_{rem}^{(L)}$ for the Lewis contribution, $J_{rem}^{(deloc)}$ for the "remote" delocalization contribution from $\sigma_{C2H1} \rightarrow \sigma_{C6H7}$* and $\sigma_{C6H7} \rightarrow \sigma_{C2H1}$*, $J_{vic}^{(deloc)}$ for the vicinal contribution from $\sigma_{C4C5} \rightarrow \sigma_{C6H7}$* and $\sigma_{C3C4} \rightarrow \sigma_{C2H1}$*, and $J_{rvic}^{(deloc)}$ for the *reverse* vicinal contribution from $\sigma_{C6H7} \rightarrow \sigma_{C4H5}$* and $\sigma_{C2C1} \rightarrow \sigma_{C3C4}$*. $J_{rvic}^{(deloc)}$ differs from $J_{vic}^{(deloc)}$ for ethane, because it results from spin density being delocalized *away* from a nucleus in the coupling pair, instead of being delocalized toward it. In general, pentane is seen to exhibit large $J_{rem}^{(L)}$ contributions and much smaller contributions from $J_{rem}^{(deloc)}$, $J_{rvic}^{(deloc)}$, and $J_{vic}^{(deloc)}$, corresponding to the weakening of hyperconjugative interactions at longer range (Table 3).

The important spatial effects of orthogonalization can be seen by comparing Figure 11A, which displays the σ_{C2H1} PNBO, and Figure 11B, which shows the σ_{C2H1} (fully orthogonalized) NBO. The additional level of orthogonality imposed on NBOs causes them to incorporate small oscillatory features (Figure 11B), which are visible even in the neighborhood of the remote H_7 nucleus. These oscillatory features can carry nuclear spin orientation information, because the orthogonalization tails of the α- and β-spin sets are affected *differently* by the presence of the perturbation. Therefore, the α- and β-spin NBOs centered at remote atoms will respond differently to the perturbed NBO

(49) Goodman, L.; Pophristic, V.; Weinhold, F. *Acc. Chem. Res.* **1999**, *32*, 983−993.

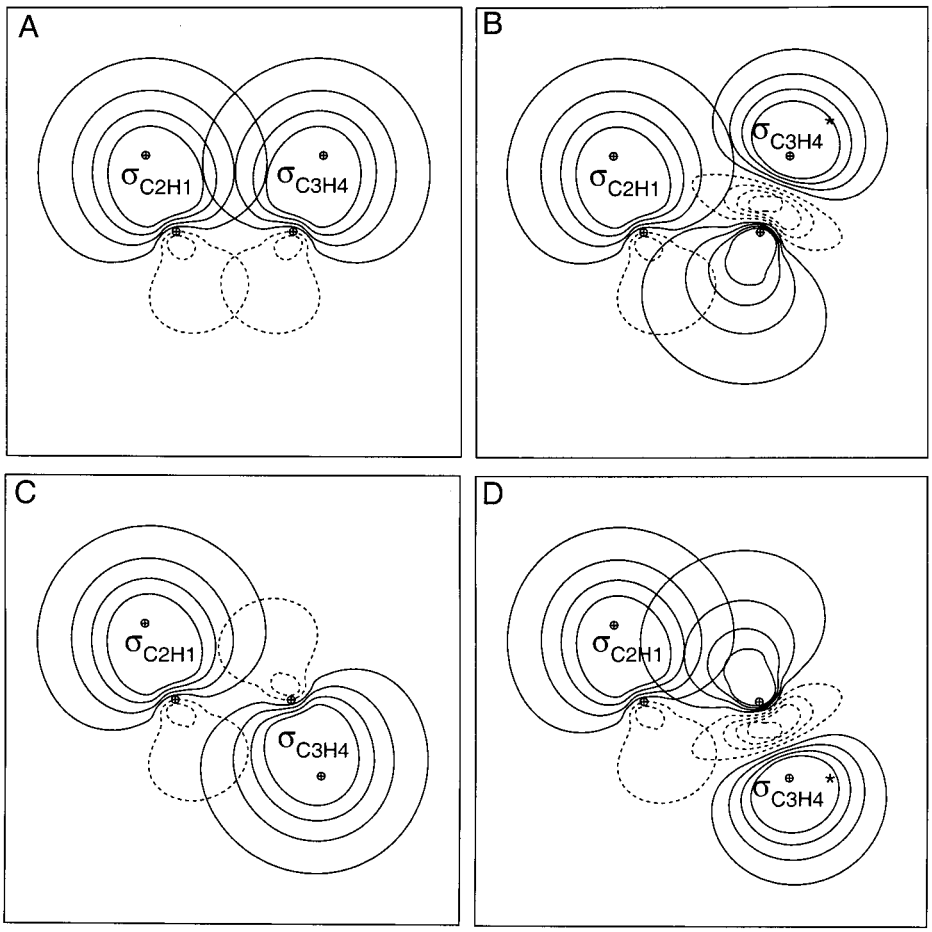

Figure 9. Prenatural bond orbital (PNBO) contours: A. σ_{C2H1} and σ_{C3H4} for cis ethane. B. σ_{C2H1} and σ_{C3H4}* for cis ethane. C. σ_{C2H1} and σ_{C3H4} for trans ethane. D. σ_{C2H1} and σ_{C3H4}* for trans ethane.

Table 2. Summary of the Calculated Contributions to Vicinal $^3J_{HH}$ Coupling of the Trans Ethane Model (Figure 1B)[a]

	D95	6-31+G*	cc-pVDZ	6-311G**	6-311++G**	aug-cc-pVDZ	cc-pVTZ
basis functions	32	50	58	72	86	100	144
$J_{vic}^{(L)}$ (/Hz)	11.34	11.44	9.80	11.04	12.58	9.04	10.92
$J_{vic}^{(deloc)}$ (/Hz)	6.56	5.64	4.52	5.26	5.08	5.78	5.62
others (/Hz)	−1.89	−1.90	−2.39	−1.88	−2.68	−2.12	−1.12
total (/Hz)	16.01	15.18	11.93	14.42	14.98	12.70	15.42

[a] Calculations performed using the B3LYP density functional at the basis listed, with a Fermi contact spin perturbation of 0.02 au.

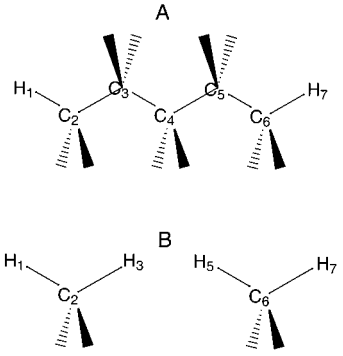

Figure 10. Pentane model.

tails that pass through them, and these Pauli-preserving responses can evidently give rise to nonzero spin density at the remote atom. In other words, the nodal features resulting from exchange antisymmetry, at or near other atoms in the molecule, can serve as an indirect means by which spin density can be transferred throughout the molecule. In this way, steric exchange antisymmetry can have longer-range consequences than hyperconjugation, given the potential for a cascade of Pauli-preserving spatial adjustments of (high-occupancy) Lewis NBOs and direct communication by orthogonalization tails.

The fact that the spin orbitals decay exponentially might suggest that long-range coupling is simply a through-space phenomenon and that the intervening atoms are mere spectators. To test this supposition, we created a dimethane model of pentane (Figure 10B) by removing C_3, C_4, and C_5 and their attached protons, and by replacing C_3 and C_5 by protons (using appropriate C−H bond lengths), and then recomputed the coupling between protons H_1 and H_7. Without the intervening carbons in the *n*-pentane chain, the calculated coupling was found to be negligibly small for all basis sets employed (see Table 3 for a list of basis sets used in the calculations). This result indicates that the intermediate carbons *do indeed play an important role* in coupling transferred through the steric exchange mechanism. In Figure 12, the PNBO and NBO forms of the σ_{C2H1} orbital are shown for the dimethane model (Figures

Table 3. Summary of the Calculated Contributions to $^6J_{HH}$ Coupling in the Trans *n*-Pentane Model (Figure 10)[a]

	D95	6-31+G*	cc-pVDZ	6-311G**	6-311++G**	aug-cc-pVDZ	cc-pVTZ
basis functions	74	119	130	162	194	223	318
$J^{(L)}_{rem}$ (/Hz)	0.20	0.22	0.18	0.22	0.26	0.16	0.22
$J^{(deloc)}_{rem}$ (/Hz)	0.02	0.06	0.06	0.04	0.02	0.02	0.04
$J^{(deloc)}_{vic}$ (/Hz)	0[b]	0.02	0.04	0[b]	0.02	0[b]	0[b]
$J^{(deloc)}_{rvic}$ (/Hz)	0.04	0.04	0.04	0.04	0.04	0.06	0.04
others (/Hz)	0.02	−0.01	−0.09	−0.01	0.05	0	−0.02
total (/Hz)	0.28	0.33	0.23	0.29	0.29	0.24	0.28

[a] Calculations performed using the B3LYP density functional at the basis listed, with a Fermi contact spin perturbation of 0.02 au. [b] Contribution is smaller than 0.01 Hz. Other small contributions can appear but are not persistent over all basis sets.

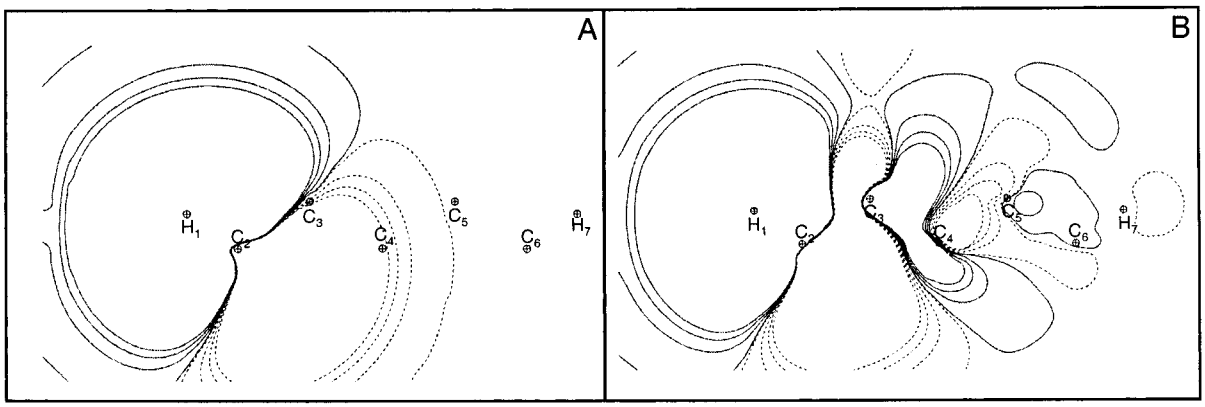

Figure 11. Two-dimensional contour plots of natural bond orbitals (NBOs) and prenatural bond orbitals (PNBOs) in the pentane model (Figure 10). A. σ_{C2H1} PNBO. B. σ_{C2H1} NBO.

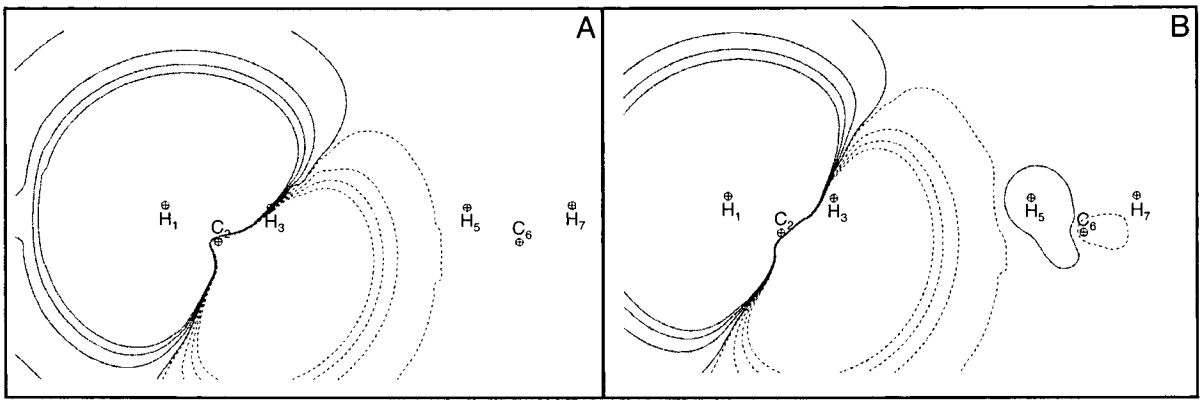

Figure 12. Two-dimensional contour plots of the natural bond orbitals (NBOs) and prenatural bond orbitals (PNBOs) in the dimethane model. A. σ_{C2H1} PNBO. B. σ_{C2H1} NBO.

12A and 12B respectively). As expected, the form of the PNBO shown in Figure 12A is quite similar to that shown in Figure 11A. However, the form of the NBO in Figure 12B differs substantially from that of Figure 11B in that it exhibits many fewer nodal features. In addition, no contours appear in the vicinity of H_7. Therefore, it can be concluded that the intermediate bonds in *n*-pentane serve to relay the *J*-coupling information down the alkane chain through a cascade of Pauli-preserving adjustments. This result is consistent with the conclusions of Del Bene et al.,[15] who found that O−H−O trans-hydrogen-bond coupling decreases when the intermediate proton is removed. This emphasizes that wave function antisymmetry is an *N*-electron phenomenon involving *all* electron pairs (including core pairs), not just those in closest "steric contact" (as judged, e.g., by empirical van der Waals radii). However, despite the fact that coupling transferred by means of steric exchange is not simply related to spatial distance, it can be expected to still exhibit a exponential-like distance relationship when the molecular environments are truly comparable (as has been shown, for example, with F−F couplings[50]).

V. Conclusion

Although steric contact is clearly important, it should be noted that other factors, including orbital occupancy and hybridization, significantly affect the sign and magnitude of *J*-coupling constants. In particular, NBOs with high s-character (i.e., σ and σ^* NBOs) have a much greater significance, because of the nonzero amplitude at their origins. In addition, core orbitals, which normally are not (directly) involved in determining chemical properties, can also be a factor in heavy-atom coupling. Ultimately, all of these factors are interdependent.

(50) Mallory, F. B.; Mallory, C. W.; Butler, K. E.; Lewis, M. B.; Xia, A. Q.; Luzik, E. D.; Fredenburgh, L. E.; Ramanjulu, M. M.; Van, Q. N.; Francl, M. M.; Freed, D. A.; Wray, C. C.; Hann, C.; Nerz-Stormes, M.; Carroll, P. J.; Chirlian, L. E. *J. Am. Chem. Soc.* **2000**, *122*, 4108−4116.

The NJC analysis demonstrates how *J*-couplings can be decomposed into individual and pairwise localized NBO contributions. Owing to the inherent compact nature of the NBO basis, nearly all of the *J*-coupling can be accounted for by a few individual and pairwise NBO contributions, regardless of the size of the basis. The resulting contributions can then be further related to other wave function properties, such as steric and hyperconjugative delocalization energies, in addition to natural charges (natural population analysis), natural resonance structures and bond orders (natural resonance theory), and natural chemical shift tensor elements (natural chemical shielding). For example, trans-hydrogen-bond $^{3h}J_{NC'}$ couplings in peptides have been shown to be strongly correlated with their corresponding H^N chemical shifts.[12] Information on the physical basis for this correlation could be obtained by comparing natural chemical shielding tensor elements to *J*-coupling contributions, to determine which specific interactions are responsible for the mutual dependence. NJC can provide a useful, comprehensive view of how coupling is propagated through a molecule that can be used to understand and predict coupling strengths on the basis of specific, localized chemical features.

Appendix

The Fermi contact spin density contributions from each NLMO can be broken down, by means of the α- and β-spin NBO to NLMO transformation matrices, into contributions from their constituent NBOs, so as to obtain more detail about individual and pairwise NBO interactions involved in coupling. The Fermi contact spin density from the *parent* NBO (i.e., $J_i^{(L)}$) for NLMO Ω_i^α on nucleus N is given by

$$\Delta_{ii}^\alpha = \langle \sigma_i^\alpha | \delta(r_N) | \sigma_i^\alpha \rangle \tag{A1}$$

and the corresponding delocalization contributions (i.e., $J_i^{(deloc)}$ and $J_i^{(repol)}$) are

$$\Delta_{ij}^\alpha = [c_{ji}^\alpha]^2 [\langle \sigma_j^\alpha | \delta(r_N) | \sigma_j^\alpha \rangle - \langle \sigma_i^\alpha | \delta(r_N) | \sigma_i^\alpha \rangle] + 2c_{ii}^\alpha c_{ji}^\alpha \langle \sigma_i^\alpha | \delta(r_N) | \sigma_j^\alpha \rangle + \sum_k c_{ji}^\alpha c_{ki}^\alpha \langle \sigma_j^\alpha | \delta(r_N) | \sigma_k^\alpha \rangle \tag{A2}$$

where c_{ji}^α is the *ji*th element of the σ^α to Ω^α transformation matrix, and $k \neq j \neq i$. Therefore, the total α-spin density associated with NLMO Ω_i^α is

$$\Delta_i^\alpha = \sum_j \Delta_{ij}^\alpha = \langle \Omega_i^\alpha | \delta(r_N) | \Omega_i^\alpha \rangle \tag{A3}$$

with analogous equations for the β-spin orbitals. From eq A3, the net Fermi contact spin density can be computed term by term for each NBO donor−acceptor interaction by simply taking the difference of the corresponding α- and β-spin values

$$\Delta_{ij} = \Delta_{ij}^\alpha - \Delta_{ij}^\beta \tag{A4}$$

in order to determine which specific donor−acceptor interactions are contributing to the spin density.

Because this method involves applying a single perturbation on one atom in a model and observing a response at another atom in the molecule, one can only gain insight into how spin density is transferred from the perturbed atom to the observed atom, but not the reverse. To remedy this and restore the physical symmetry of spin coupling, an additional calculation is performed on the identical model system in which the roles of the "perturbed" and "observed" nuclei are reversed. Individual spin density contributions from each calculation are then averaged to yield

$$[\Delta]_{ij} = \frac{[[\Delta(r_M)]_{ij}]_{\lambda_N} + [[\Delta(r_N)]_{ij}]_{\lambda_M}}{2} \tag{A5}$$

where $[[\Delta(r_M)]_{ij}]_{\lambda_N}$ refers to the spin density evaluated at the position of atom M, with the perturbation applied to atom N.

In certain cases, it can happen that an NLMO contribution Ω_i can contain a non-negligible delocalization contribution involving another (high-occupancy) Lewis NBO σ_j, resulting in a donor−donor interaction instead of donor−acceptor. This occurs as a result of the procedure for constructing the NLMOs. As shown in eq 2, each NLMO Ω_i is constructed from a linear combination of NBOs, with a single parent Lewis NBO σ_i. However, it is possible in rare cases that a different Lewis NBO σ_j can have a nonzero coefficient c_{ji}, thus resulting in a donor−donor interaction with σ_i. If such a situation results in nonnegligible spin density delocalization contribution, NJC will move the spin density contribution from the Ω_i NLMO to the Lewis category of NLMO Ω_j. Doing so removes the physically undesirable donor−donor interaction, while maintaining accountability for all of the spin density contributions.

Acknowledgment. This work was supported in part by NIH grant RR02301 from the Biomedical Research Technology Program of the National Center for Research Resources, National Institutes of Health. S.J.W. was supported in part by a traineeship from an NIH Molecular Biophysics Training Grant (GM08293). Software development and computations were carried out on a four-processor server graciously donated to the University of Wisconsin National Magnetic Resonance Facility (NMRFAM) by the Microsoft Corporation.

JA016284K